Customised production of injection moulded parts from recycled materials using rapid tooling approach and coupled injection moulding-thermal and mechanical simulation

Krizsma Sz. G., Suplicz A., Gere D.

Results in Engineering 26 (2025) 105272

Contents lists available at ScienceDirect

Results in Engineering

journal homepage: www.sciencedirect.com/journal/results-in-engineering

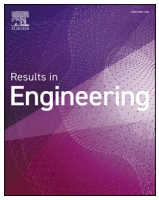

Research paper

Customised production of injection moulded parts from recycled materials using rapid tooling approach and coupled injection moulding-thermal and mechanical simulation

Szabolcs Krizsma [a,b,*], András Suplicz [a,b], Dániel Gere [a]

[a] Department of Polymer Engineering, Faculty of Mechanical Engineering, Budapest University of Technology and Economics, Műegyetem rkp. 3., H-1111, Budapest, Hungary
[b] MTA-BME Lendület Lightweight Polymer Composites Research Group, Műegyetem rkp. 3., H-1111, Budapest, Hungary

ARTICLE INFO

Keywords:
Rapid tooling
Recycled materials
Circular economy
Material jetting
Injection moulding simulation
Coupled simulation

ABSTRACT

Additive manufacturing is the state of the art in modern tool making. It makes the low-volume production of polymeric parts and prototype moulds feasible. Injection moulded parts can be customised flexibly and fast with prototype polymeric moulds. Another trend in the plastics industry is the widespread use of recycled materials to reduce environmental impact. In this article, we introduce a novel technological concept: applying prototype injection moulds to process recycled materials. We investigated three materials: original PP, a recycled PP-HDPE mixture, which is a commercially available injection moulding material and a recycled PA6 that is difficult to mould due to the high melt temperature. All three materials were injection moulded successfully with outstanding product quality. The injection moulding process was modelled with a coupled injection moulding simulation—finite element thermal and mechanical simulation. The presented novel modelling method proved accurate. The injection pressure, temperature and strain results of the simulations showed excellent agreements with the measured results. The application of additively manufactured prototype moulds to produce parts from recycled materials is definitely a novelty.

1. Introduction

The plastics industry today is driven by several global trends. Significant trends include the rise of additive manufacturing, the emerging demand to recycle plastics and the wider application of digitization and automation. These trends are driven by the need to increase efficiency, and reduce costs and the environmental impact.

Additive manufacturing (AM) has already revolutionised part and tool making. With AM, injection moulds can be produced fast and cost-effectively in a single technological step. This application of AM is called direct rapid tooling (RT) which reduces the significant investment cost and lead time of conventional mould machining. Therefore, the hybridization of injection moulding with additively manufactured moulds and part inserts has the potential to deliver outstanding results both from an engineering and an economic point of view. The flexibility of AM also allows the mass customisation and cost-effective low-volume production of injection moulded parts. This flexibility is essential for injection moulding to adapt to rapidly changing customer needs. The most popular polymeric additive technologies in low-volume mould making are typically photopolymer resin–based: stereolitography (SLA), material jetting (MJ) and digital light projection (DLP). The main factors that influence printing quality are build layer thickness, degree of curing, density of the polymerised material, and possible post-curing methods. Polymeric low-volume moulds have already appeared in injection moulding. Case studies available on their application are typically limited to feasibility studies and the maximum number of cycles.

Rahmati and Dickens [1] printed injection mould cavity insert shells by stereolitography (SLA) from an epoxy resin. They filled these shells with aluminium-filled epoxy resin to increase their stiffness and thermal conductivity. They measured the operational cavity pressure and temperature of the mould inserts and analysed their failure mechanism. Insert failure occurred after 500 injection moulding cycles. They also concluded that melt temperature fundamentally influences the lifetime of the mould inserts. Walsh et al. [2] tested the dimensional stability of SLA printed parts. They found that a scaling factor of 109.3 % was necessary to reach nominal dimensions. They concluded that the main

* Corresponding author.
E-mail address: krizsmasz@pt.bme.hu (S. Krizsma).

https://doi.org/10.1016/j.rineng.2025.105272
Received 25 February 2025; Received in revised form 29 April 2025; Accepted 9 May 2025
Available online 15 May 2025

material parameters determining the suitability of the material for prototype injection moulds are tensile strength, elongation at break and heat deflection temperature. Davoudinejad et al. [3] analysed the effect of thermal aging on the lifetime of SLA-printed mould inserts. They injection moulded ABS into two inserts which were in their as-printed state, and four inserts which were subjected to thermal aging. During thermal aging, the temperature of the mould inserts varied cyclically between 23 °C and 100 °C for 6 h. Heating speed was 5 °C/min. The treated inserts were subjected to 20 thermal cycles and were left for 2 weeks at room temperature. Cracks appeared on the untreated inserts at 70 and 95 cycles while the thermally aged inserts started cracking at 50, 30, 12 and 8 cycles. The results indicated that cyclic thermal loads (thermal aging) have a negative effect on the lifetime of SLA-printed mould inserts. Giorleo et al. [4] printed injection mould inserts by material jetting (MJ) from a high-temperature (HT) resin. They showed that the printing orientation has a significant effect on the surface quality of the inserts as well as their failure. They also found that the inserts produced by MJ are suitable for micro injection moulding, due to the small build layer thickness and the resulting dimensionally accurate printing. Bogaerts et al. [5] also produced injection mould inserts from DigitalABS resin by MJ. They found that high-temperature zones occur on the mould inserts during operation, due to the cyclically injected hot polymer melt. The location and the extent of these high-temperature zones determine the lifetime of the polymeric mould inserts. Due to this, they recommend the application of thermal imaging camera measurements to monitor mould insert temperature to increase their lifetime. Bagalkot et al. [6] presented the typical failure mode of MJ-printed polymeric moulds. The first step of failure is the appearance of microcracks and thermal degradation of the surface. The second step is crack propagation and the resulting delamination. These are caused by the shear load or the bending load created by the high-pressure injected melt. Stampone et al. [7] also applied MJ to manufacture mould inserts from a HT resin. The injection moulded material was poly(methyl methacrylate) (PMMA), which has to be processed at high temperature and pressure. They found that small geometrical features (that are necessary for micro injection moulding) drastically promote crack initiation especially for rigid materials like a HT resin, which exhibits glass-like behaviour in the application temperature range. However, when no sharp notches were present, the flat mould inserts withstood 50 moulding cycles without any problems. Bagalkot et al. [8] identified mould temperature, injection pressure and injection speed as the critical process parameters that determine the lifetime of MJ-printed polymeric mould inserts. Berges et al. [9] applied material extrusion to print a prototype polymeric mould insert, which they used successfully for metal injection moulding.

Mendible et al. [10] compared three injection mould inserts manufactured by conventional machining, MJ and direct metal laser sintering (DMLS). The inserts were produced from stainless steel, Digital ABS and bronze, respectively. The bronze and the stainless steel inserts showed similar operational behaviour and product quality. The metallic inserts were used for 500 moulding cycles without observable tool wear. On the other hand, the parts made with the Digital ABS mould insert were defective after 80 cycles and the mould insert cracked at 116 cycles. The PolyJet insert also cooled significantly slower, which caused increased product shrinkage and a higher degree of crystallinity of the moulded products. Mendible et al. [11] also compared polypropylene (PP) tensile test specimens injection moulded into an aluminium and a PolyJet-printed, Digital ABS injection mould. They found that the specimens injection moulded into the Digital ABS mould showed approximately 30 % higher modulus of elasticity and significantly lower elongation at break. This embrittlement of the parts was caused by the slower heat extraction of the Digital ABS mould and the resulting higher degree of crystallinity in the tensile specimens. Kampker et al. [12] presented a similar comparative study and had similar conclusions. They also analysed high-performance thermoplastic mould materials (PA3200GF – reinforced PA12, printed by selective laser sintering). Tábi et al. [13] also compared the mechanical and thermal properties of poly (lactic acid) (PLA) plates injection moulded into a conventional steel mould and a PolyJet printed mould insert. The parts injection moulded with the PolyJet insert exhibited considerably higher crystallinity compared to the parts produced with the steel mould. This difference in crystallinity is primarily caused by the two orders of magnitude lower thermal conductivity of the Digital ABS compared to tool steel. As a result of this lower thermal conductivity cooling time is considerably longer, which is beneficial for the crystallisation of PLA.

Nowadays, the use of recycled materials in plastic products is gaining more and more attention. This is due to various European Union directives and regulations (e.g. 2025/40, 2018/852, and 2022/1616) on the one hand, and social expectations and marketing considerations on the other [14–16]. With recycled materials, compromises must be made in many cases, for example, mechanical properties or visual appearance can be impaired [17,18]. Additive manufacturing can be a good method for testing recycled materials, as in addition to visually inspecting the products, functional tests can also be performed [19]. One solution could be to print the product using filaments made from recycled materials [20,21]. Innovative and successful projects have produced filaments for AM from recycled plastics [22,23]. Another solution could be to injection mould recycled plastics into additively manufactured inserts, like in our research. The use of recycled plastics can be particularly beneficial with additively manufactured inserts because the increased flowability of recycled plastics due to reduced molecular weight reduces the thermal and mechanical degradation of the insert, which extends its lifetime [8,17]. Additionally, there are methods for adjusting injection moulding parameters to increase insert life [24,25].

Alongside the rise of AM in mould making and the increase in the amount of recycled materials, another development direction is digitization, automated process and product quality control, and the application of modern measurement technology, which is still not fully elaborated. However, the application of sensor technology helps to adjust the injection moulding parameters relatively fast and product quality can be optimal. The use of sensors also allows real-time process supervision, which can increase the lifetime of injection moulds. In industrial practice, the use of sensors is typically limited to cavity pressure measurement. However, operational temperature and strain measurement also yields valuable data that can be used to control the injection moulding process. Ageyeva et al. [26] summarised the wide range of available measurement technologies, including temperature and pressure sensors. Zhao et al. [27] also made a comprehensive review on the application of different measurement techniques in injection moulding. Chen et al. [28] propose to measure the elongation of the injection moulding machine tie bars for the continuous adjustment of the switchover point (from filling to holding) during production. From the variation in the elongation of the column, they inferred the fluctuation of clamping force based on Hooke's law. It has significant practical relevance, as clamping force fluctuation has a profound effect on product quality. Insufficient clamping force leads to flash, while too high a clamping force leads to increased tool wear and poor ventilation during moulding. Mahshid et al. [29] placed inductive sensors on the fixed and the moving side mould plates and measured mould deformations with an accuracy of approximately 10 μm. Huang and Lin [30] measured the deformation of the tie bars of the injection moulding machine and used the measured values to estimate the minimally required clamping force. They also outlined an algorithm to set the ideal clamping force based on the measured elongations. Gülcür et al. [31] applied the combination of computer tomography (CT) and confocal laser scanning microscopy (CLSM) to analyse the dimensional variations of micro injection moulded parts. They used a PolyJet-printed injection mould insert made from Vero PureWhite (RGD837) photopolymer resin. They characterised the gradual wear of the mould inserts by the analysis of the geometrical features on the mould inserts. Their measurement system can track the dimensional variations of the products moulded by the photopolymer inserts. Baruffi et al. [32] also analysed the micro

injection moulding process with a high-speed thermal imaging camera in a special mould with a window on it. They used the thermal imaging camera images to optimise the moulding parameters and the resulting product quality. Guerrier et al. [33] also used a special mould with a glass window to monitor the cavity filling stage with a high-speed camera and used the images to optimise the filling parameters.

The application of numerical methods, mostly finite element simulation has already boosted product development and mould design. Injection moulding simulation allows the optimisation of product geometry, moulding parameters and also the cooling system layout [34,35]. Slama et al. [36] presented a methodology to design optimal conformal cooling channels for a mould using cooling simulation in Autodesk Moldflow. Cervantes-Vallejo et al. [37] presented a coupled simulation approach to optimise the positions of the heating cartridges and the cooling channels in rapid heat cycle moulding (RHCM). The pressure load acting on the mould was calculated with a Moldex3D injection moulding simulation. Then they used this pressure load in a coupled thermo-mechanical simulation in Ansys Workbench. They used their model to optimise the operational thermal state of the mould to reduce the required time to heat and cool the mould during the cycle. They also minimised the operational stresses in the mould plates to increase the lifetime of the mould. Crema et al. [39] analysed mould inserts with lattice structures because the porous inserts allow the direct circulation of the coolant water in the entire mould volume. This is especially beneficial for RHCM. They created a coupled computational fluid dynamics (CFD) and structural simulation model to analyse the operational deformation and the stress state of the porous mould insert. They validated their model with actual injection moulding tests, using the measured temperature–time curves. Macedo et al. [38] analysed the connection between the moulding parameters and the thickness of the frozen layer of specimens injection moulded into an RHCM mould. Wang et al. [40] applied RHCM to eliminate weld lines and improve the surface quality of an automotive part. They analysed the position of the weld lines by injection moulding simulation (Autodesk Moldflow) and simulated the operational temperature distribution of the mould block in Ansys Workbench. They optimised the positions and the dimensions of the baffles to make the temperature of the cavity surface as uniform as possible. They also performed injection moulding tests with the optimised mould design and found adequate agreements between the measured temperatures and the simulation results. Xiao and Huang [41] also used transient thermal analysis (in Ansys Workbench) to model the thermal state of an injection mould equipped with RHCM. They validated their thermal model with thermal imaging camera images during the injection moulding cycles. Following the successful validation of the thermal model, they created a coupled mechanical simulation to model the thermal stresses occurring during the RHCM cycle. Based on their mechanical model, they redesigned the fixing of the cavity inserts, reducing the service stresses in the critical areas of the inserts and increasing the lifetime of the inserts. Li et al. [42] analysed the failure of an injection mould fitted with electric heating cartridges. The cyclically occurring thermal stresses caused early failure of the mould. The coupled thermo-mechanical simulation also showed the actual failure location as the critical area, proving the adequacy of the thermo-mechanical simulation in the analysis of injection moulds. Guerrier et al. [43] applied thermal simulations to model the thermal state in an induction-heated injection mould. They used injection moulding simulation (Moldex3D) and thermal simulation (Ansys)

A good amount of knowledge has been acquired about the applicability of prototype polymeric moulds but a comprehensive use of sensors and modelling of these inserts is extremely rare. The simultaneous measurement of operational deformation and temperature gives valuable insight into the operational characteristics of polymeric moulds. The concept of using additively manufactured low-volume moulds to process recycled materials is a novelty and it has outstanding practical relevance as the need to achieve a circular economy is growing stronger every day. This article also shows how a coupled simulation approach, combining injection moulding simulation with finite element thermal and mechanical simulation, can model the operational behaviour of polymeric prototype mould inserts. For such a coupled model, the properties of the mould insert material have to be determined first. The temperature-dependent stiffness of the material was measured by conventional dynamic mechanical analysis (DMA) and the creep properties were also measured by DMA in creep time temperature superposition (TTS) mode. After the material tests, the actual injection moulding experiments were performed with the different recycled materials. Operational strain, temperature, cavity pressure and injection (machine) pressure were measured during the injection moulding tests. These measured curves also served as validation tools for subsequent finite element modelling. After the moulding tests, we performed the coupled injection moulding simulation, and finite element thermal and mechanical simulations. The finite element models were validated successfully with the measured injection pressure, temperature and strain curves. Our results prove that recycled materials can be processed with low-volume moulds, which can be manufactured easily and flexibly, and also that the injection moulding process can be systematically designed with the coupled simulation approach.

2. Materials and methods

2.1. Preparation of mould insert and samples

Dynamic mechanical analysis (DMA) specimens were printed from RGD835 VeroWhite (epoxy-acrylate) resin produced by Stratasys Ltd. (United States). The inserts were printed with an Objet Alaris 30 printer manufactured by Stratasys. The dimensions of the specimens were 4 mm × 10 mm × 59 mm for the three-point bending arrangement and 4 mm × 10 mm × 50 mm for the dual cantilever arrangement (based on ISO 6721). The mechanical and thermal properties of VeroWhite are presented in Table 1.

2.2. Material testing

The printed specimens were analysed with a TA Instruments (USA) Q800 dynamic mechanical analyser (DMA). The DMA analysis determined the creep compliance at different temperatures (in creep time temperature superposition (TTS) mode). Table 2 shows the test parameters. The analysed temperature range was chosen to completely cover the application temperature range of the mould insert. The creep parameters were measured in three-point bending arrangement.

The temperature dependence of stiffness was also measured by DMA in multi-frequency–strain mode and the tests were performed with the dual cantilever clamp. The analysed temperature region was 25–105 °C, and the loading frequency was 1 Hz. Heating speed was 3 °C/min and the amplitude of loading was 15 μm. The amplitude and the frequency of the load were chosen to be in the linear viscoelastic region.

The specific heat capacity of the injection moulded materials (recycled PP-HDPE mixture and recycled PA6) were measured by modulated differential scanning calorimetry (MDSC) on a DSC Q2000 (TA Instruments, USA) device. It is crucial to determine the specific heat

Table 1
Material properties of RGD835 VeroWhite.

Properties	Unit	Typical value
Tensile strength	MPa	50–65
Flexural strength	MPa	75–110
Modulus of elasticity	GPa	2–3
Elongation at break	%	10–25
Heat deflection temperature (0.45 MPa)	°C	45–50
Thermal conductivity	W/(m·K)	0.2
Specific heat	J/(kg·K)	1200–2640 (20 °C–100 °C)
Coefficient of thermal expansion	1/K	~75·10^{-6}

Table 2
Parameters of DMA creep TTS testing.

Parameters used	Unit	Typical value
Furnace time	min	10
Creep time	min	30
Recovery	min	30
Minimum temperature	°C	30
Maximum temperature	°C	65
Temperature increment	°C	5
Bending stress	MPa	5
Atmosphere	Air	

capacity of the moulded materials exactly so that the heat load transferred to the mould insert during the cooling of the product can be accurately modelled.

2.3. The comprehensive measurement system of the injection mould insert

Fig. 1 shows the test mould. The dimensions of the injection mould insert were 75 mm × 65 mm × 15 mm. The injection moulded product was a ring with an average diameter of 44 mm. The mould was filled through two standard gates. The gate inserts were also made from RGD 835 (VeroWhite). The measurement system of the prototype mould contains a strain gauge (KMT-LIAS-06–3–350–5EL, Hungary) glued into the slot at the back of the insert. The temperature of the mould insert was measured with a thermowire (Ahlborn NiCr-Ni thermowire T 190–0, Ahlborn Mess- und Regelungstechnik GmbH, Germany) also glued to the back of the insert in the respective hole. Cavity surface temperature was measured with a FLIR A325sc thermal imaging camera (Teledyne FLIR LLC, Wilsonville, United States). The measured strain data were collected with a Spider 8 unit (Hottinger Baldwin Messtechnik GmbH, Austria), while the temperature data were gathered with an Ahlborn Almemo 8990–6 data collector unit (Ahlborn Mess- und Regelungstechnik GmbH, Germany). The accuracy of the injection moulded products was checked by 3D scanning, with a GOM ATOS Core 5 M scanner (Carl Zeiss GOM Metrology GmbH, Germany) whose theoretical resolution is 0.01 mm.

We used three different materials. The first one was an original polypropylene homopolymer (Tipplen H145F) manufactured by MOL Group Plc. (Hungary). It has a low minimal recommended processing temperature (230 °C) and an excellent melt flow index

(MFI=29 g/10 min at a load of 2.16 kg). The second was a recycled, post-consumer cap waste (polypropylene (PP) and high density polyethylene (HDPE) mixture in 20 %–80 % ratio, MFI=12 g/10 min at 230 °C; 2.16 kg). The third material was recycled, post-industrial polyamide 6 (PA6) textile waste (MFI=200 g/10 min at 275 °C; 5 kg). After injection moulding 10 cycles with each material, we also tried to injection mould recycled post-consumer poly(ethylene terephthalate) (PET) bottle waste but the mould insert failed in the first cycle. The products were injection moulded with an Arburg Allrounder Advance 270S 400–170 (ARBURG GmbH, Germany) machine (screw diameter: 30 mm). The main injection moulding parameters are shown in Table 3 for the three materials that were injection moulded successfully. It is necessary to set a low injection rate and pressure limit to avoid a severe pressure load that could damage the mould insert. With a low injection rate, clamping force can also be reduced, which increases the lifetime of the mould insert. The low thermal conductivity of the epoxy-acrylate mould insert material also means that residual cooling time is longer, which is necessary for the product to reach a proper ejection temperature. A long idle time between the cycles is also necessary for the mould insert to cool down and this way, early failure can be prevented. During the injection moulding test, 10 cycles were moulded successfully with each material in Table 3.

2.4. Finite element modelling of the operational state of the mould insert

After the injection moulding tests, we performed the finite element modelling of the process—first, an injection moulding simulation model in Autodesk Moldflow, then a coupled thermal-mechanical simulation model in Ansys Workbench.

Table 3
The injection moulding parameters for the three materials.

Processing parameters	Unit	PP	HDPE-PP	PA
Clamping force	[tons]	5	5	5
Dose volume	[cm^3]	40	40	40
Injection rate	[cm^3/s]	15	18	18
Injection pressure limit	[bar]	400	450	400
Switchover point	[cm^3]	28	27	28
Holding pressure	[bar]	175	225	200
Holding time	[s]	5	5	5
Residual cooling time	[s]	30	30	30
Cycle time from mould closing to opening	[s]	~47	~ 47	~ 47
Overall cycle time (delay time included)	[s]	300	300	300
Melt temperature	[°C]	190	210	265

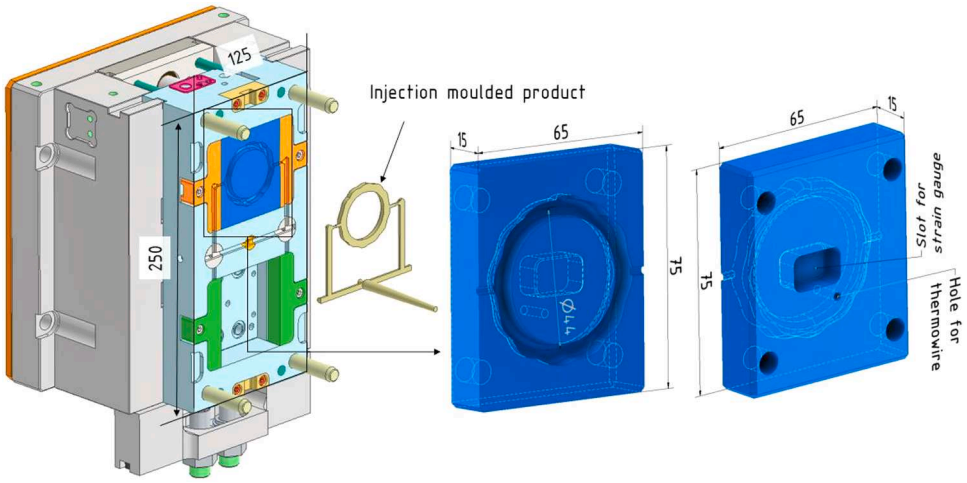

Fig. 1. The test mould, the product and the additively manufactured insert with the strain gauge slot and the thermowire hole.

3. Results and discussion

3.1. Material testing

3.1.1. Dynamic mechanical analysis

Conventional DMA was carried out first, to characterise the temperature-dependent stiffness of the mould insert material. The storage modulus (E') and the loss factor (d) were determined with the test (Fig. 2). There is a sharp drop in the storage modulus in the 35 °C to 55 °C range. The 2 GPa modulus at 35 °C drops to 0.75 GPa at 55 °C which is a 63 % decrease. The applicability of the material is mainly limited by its relatively low glass transition temperature. Therefore, it is essential to minimise the heat load on the mould insert during injection moulding. The loss factor shows a sharp peak at 70 °C, indicating the transition of the mould insert material from the glassy to the rubbery state.

3.1.2. Creep tests

Creep is a crucial source of deformation for polymeric injection moulds and inserts. The effect of creep is amplified by the elevated temperature during their operation. Creep testing was performed on DMA equipment, in creep time–temperature superposition (TTS) mode. The measured quantity was creep compliance (J), which is calculated according to Eq.(1), where (ε_{fl}) is the time-dependent flexural strain and (σ_0) is the pre-set flexural stress. Higher creep compliance indicates increased creep.

$$J(t) = \frac{\varepsilon_{fl}(t)}{\sigma_0} \tag{1}$$

Creep compliance is shown in Fig. 3. Maximum creep compliance necessarily occurs at the moment of unloading. In the lower temperature range, at 30 °C and 35 °C, the material showed glassy behaviour and the maximum creep compliance values were 1086 $\mu m^2/N$ and 1920 $\mu m^2/N$, respectively. These values indicate moderate creep in this temperature range. However, as the material enters the transition temperature region, the creep compliance changes stepwise. Maximal creep compliance was 5629 $\mu m^2/N$ at 40 °C, which is an almost threefold increase compared to the value measured at 35 °C. Above that temperature, deformation is excessive, which means that the material is not suitable for prototype moulds.

3.1.3. Measuring the specific heat capacity of the recycled materials

The measured specific heat capacity –temperature curves are presented in Fig. 4. The curves were measured during the cooling of the samples for accurate modelling of the actual injection moulding process. The recycled PA6 shows a peak in specific heat capacity at 236 °C, which corresponds to the melting temperature of the material. The recycled PP-HDPE mixture shows two peaks: one at 121 °C and one at 129 °C.

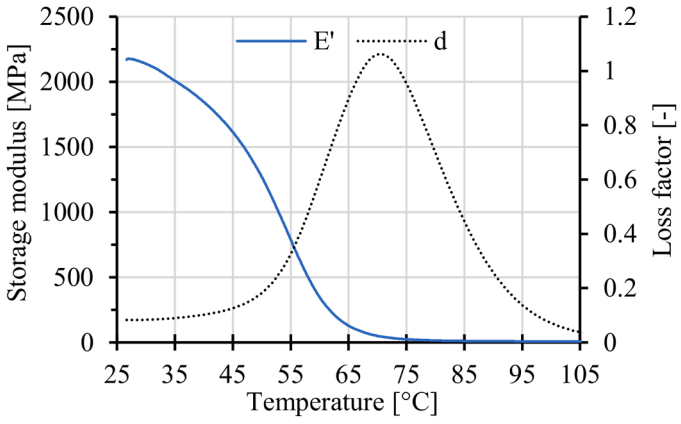

Fig. 2. Storage modulus (E') and loss factor (d) of VeroWhite (RGD835), measured by DMA.

3.2. Injection moulding tests

3.2.1. Injection moulding of original PP

The injection moulding tests were started with the original PP material. Fig. 5 shows the operational deformations of the mould insert in each cycle. The injection moulding cycle from mould closing to mould opening is detailed in Fig. 5b), while the filling and the holding phases are further detailed in Fig. 5c). A small stepwise increase can be observed at mould closing as the clamping force slightly deforms the mould insert. After that, the melt is injected at high speed and the cavity is filled through the two standard gates. This happens almost instantaneously, which results in a bigger stepwise increase in operational strain. After the volumetric filling of the cavity, the machine switches over to the holding phase. At this point, the pressure drops from the maximal injection pressure of approximately 290 bar to the pre-set holding pressure of 175 bar. This pressure drop also causes a decrease in the operational strains at switchover (indicated by the dashed bracket in Fig. 5c). Gate freeze occurs at approximately 2.2 s as the standard gate has small cross-sectional area and the aluminium cavity insert in the fixed mould half extracts the heat fast. After gate freeze, additional material can hardly be injected into the cavity in the holding phase, which results in a gradual decrease in relative strains from 5 to 7 s, until the end of the holding phase. Then, dosing occurs and the back pressure of the freshly plasticised melt compresses the runner of the moulded product (Fig. 5b). This also causes an increase in strain during dosage. After dosing is finished at 14 s, the plasticising unit with the compressed melt inside is removed from the sprue of the mould and the entire product can then cool inside the closed mould without external load. During cooling, the part shrinks, which results in free space for the mould insert to regain its original shape, and it causes a decrease in strain.

The volumetric temperature (measured by the thermowire) and the average cavity surface temperature of the mould insert (measured by the thermal imaging camera) are presented in Fig. 6a) and b), respectively. Both measured temperatures increased during the injection moulding series. Volumetric temperature varies cyclically, following the cycles, but the average temperature increases. The minimum of volumetric temperature was 26 °C at the start of the injection moulding tests, which increased to 32 °C by the 10th cycle. Average cavity surface temperature also increased from 45 °C at mould opening after the 1st cycle to 53 °C, which was measured at mould opening in the 10th cycle. The effect of the limited thermal conductivity is also presented as there is a temperature difference of approximately 20 °C between the cavity surface temperature, measured at mould opening and the maximum volumetric temperatures measured by the thermowire. It is essential to measure the heating of the polymeric mould inserts because the stiffness, the creep compliance and the thermal expansion of the material heavily depend on temperature—there is a strong correlation between insert temperature and the measured strains.

The thermal imaging camera images at mould opening with the part in the mould, right after part removal and at the end of the idle time are presented in Fig. 7a), b) and c), respectively. There is a balance between product temperature and cavity surface temperature right after product removal. Cavity surface temperature massively exceeds the glass transition temperature of the insert material. However, as a result of the low thermal conductivity of the polymeric insert material, the high-temperature zone is localised strictly around the cavity walls, which prevents the failure of the insert. After the idle time, the temperature decreases well below the glass transition range, to 27–31 °C, which is in thermal balance with the volumetric temperature measured by the thermowire.

3.2.2. Injection moulding of the PP-HDPE mixture

Fig. 8 shows the operational strains of the mould insert during the

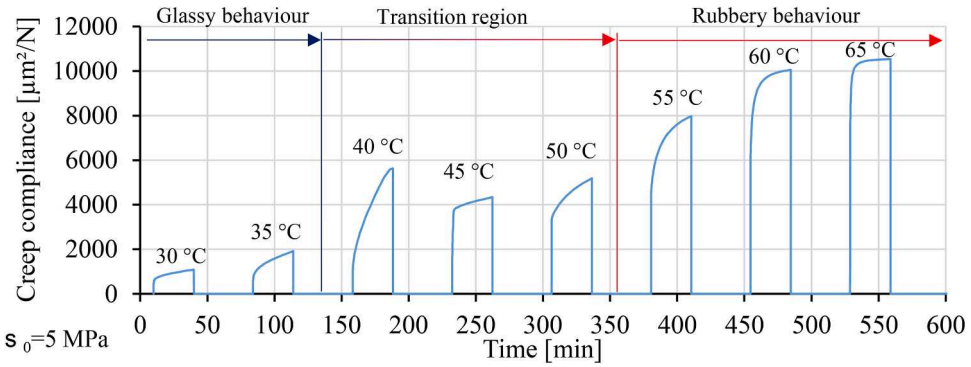

Fig. 3. Creep compliance of VeroWhite (RGD835) in the 30–65 °C temperature range measured by DMA Creep TTS.

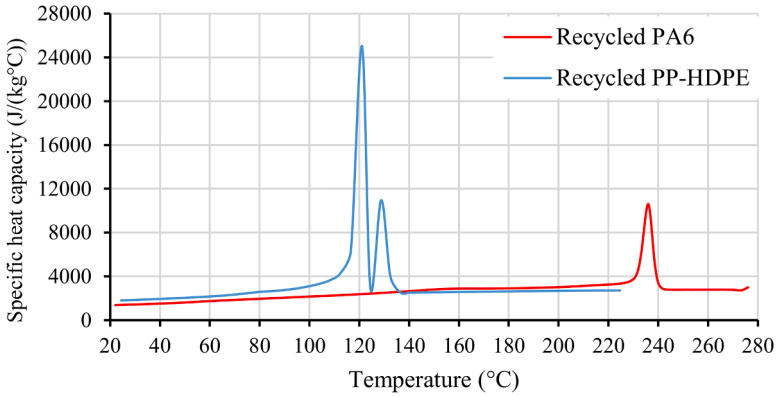

Fig. 4. Specific heat capacity of the recycled PP-HDPE mixture and the recycled PA6, measured by DSC.

injection moulding of the PP-HDPE mixture. The strain curves show a significant difference compared to the ones measured when the original PP was injection moulded (Fig. 5). It is because the viscosity of the recycled material is significantly higher than that of the original PP, which causes increased injection pressure load. There is a sharp increase in strain during cavity filling and the maximum strain at the end of filling is in the 0.08–0.13 % range, which is 2–3 times more than the strain measured when original PP was injection moulded. After switchover, the strain curves stabilise in the holding time and start to increase during dosing. Strain curves increase steadily in the residual cooling phase, because the injected melt gradually heats the mould insert. The heating of the insert causes three simultaneous phenomena. The mould insert suffers thermal expansion, the stiffness of the insert material drops while creep compliance increases significantly, amplifying the deformations at a given pressure load. The melt temperature of the PP-HDPE mixture was 210 °C compared to 190 °C of the original PP, which causes an increase in the heat load.

The volumetric temperature of the mould insert and the average cavity surface temperature are presented in Fig. 9a) and b), respectively. The insert heats up similarly to the injection moulding of original PP, but both volumetric temperature and cavity surface temperature are significantly higher. These temperature results also prove that the insert heated more intensively during the injection moulding of the PP-HDPE mixture, which is the consequence of the increased melt temperature.

3.2.3. Analysis of product quality and the failure of the inserts

The injection moulded products were 3D scanned and their dimensional accuracy was checked (Fig. 10). The shrinkage of the outer diameter can be clearly seen. The original PP material showed the highest dimensional deviation with the inner diameter varying between +0.33 and +0.50 mm. The outer diameter had a maximal deviation of −1.06 mm, which is caused by the increased shrinkage due to the relatively high wall thickness. The recycled PP-HDPE mixture showed almost the same dimensional deviations ranging from +0.33 to +0.47 mm in the inner diameter. The outer diameter showed a maximum dimensional difference of −0.86 mm, which is still relatively high. It is caused by the relatively high wall thickness and the resulting shrinkage. The recycled PA6 material is the most accurate with dimensional deviations of +0.28 to +0.33 mm in the inner diameter and −0.70 mm in the outer diameter. These results prove that products injection moulded from original and recycled materials have comparable dimensional accuracy, which means recycled materials can also be injection moulded.

Fig. 11 shows the failed gate insert and the failed cavity insert. The gate insert cracked all along the groove for the product runner. Gate insert failure happened after 10 cycles of injection moulding original PP, 10 cycles of injection moulding the recycled PP-HDPE mixture and 10 cycles of injection moulding recycled PA6 material. The cavity insert remained intact during the 30 moulding cycles. After the 30 cycles, we tried to injection mould recycled PET into the mould but it cracked instantaneously. The recycled PET remained in the mould insert (Fig. 11).

3.4. Simulation of the polymeric mould inserts

After the necessary material tests and the injection moulding series with the different materials, we used a novel coupled simulation approach to model the operational behaviour (temperature distribution and deformations) of the prototype mould inserts. Fig. 12 shows the flowchart of the coupled simulation method. The workflow starts with an injection moulding simulation (in Autodesk Moldflow), where the mould block and product geometry are meshed. The process parameters (flow rate, switchover point, mould temperature, melt temperature, holding pressure, holding time and residual cooling time) are also set at this point. After the injection moulding simulation, the mould mesh and

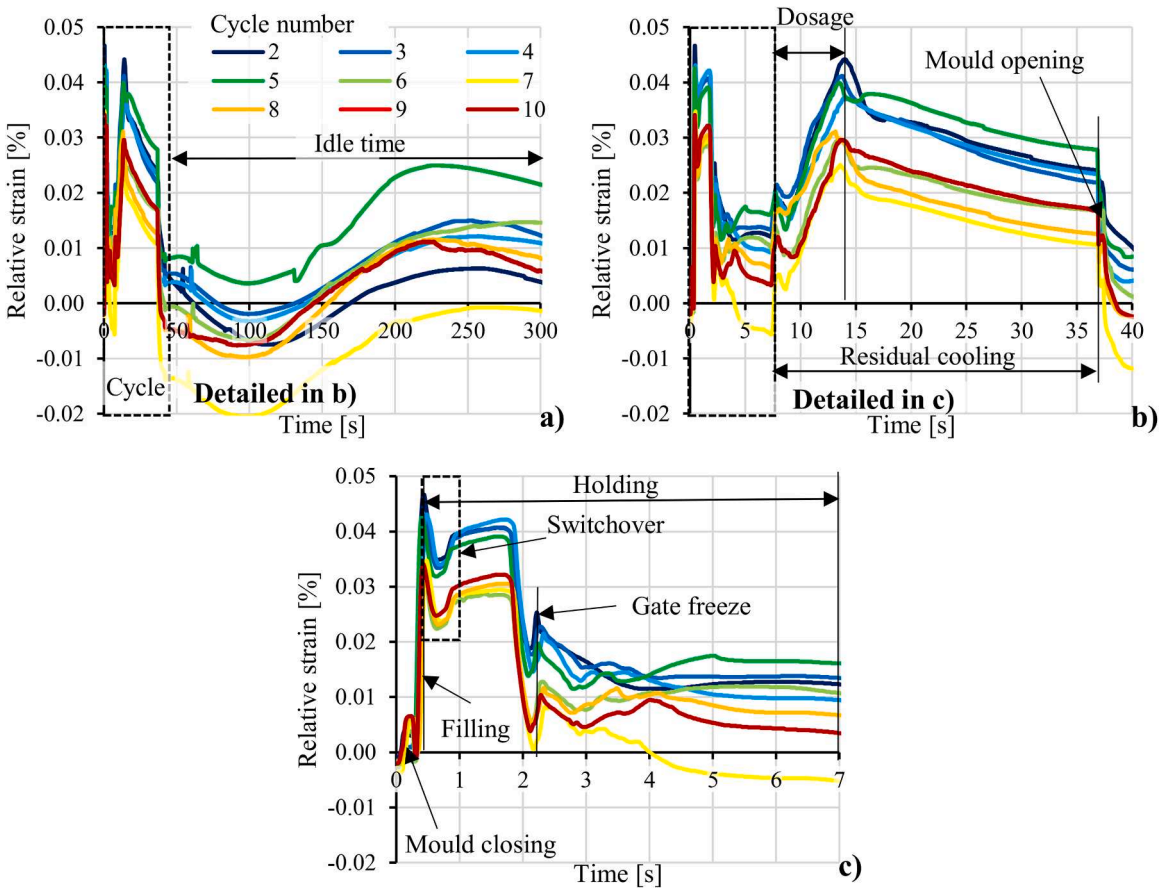

Fig. 5. Operational strain of the mould insert during the injection moulding of original PP material. Complete cycle (with delay time) a), injection moulding cycle from mould closing to part ejection b) and the filling–holding phase c).

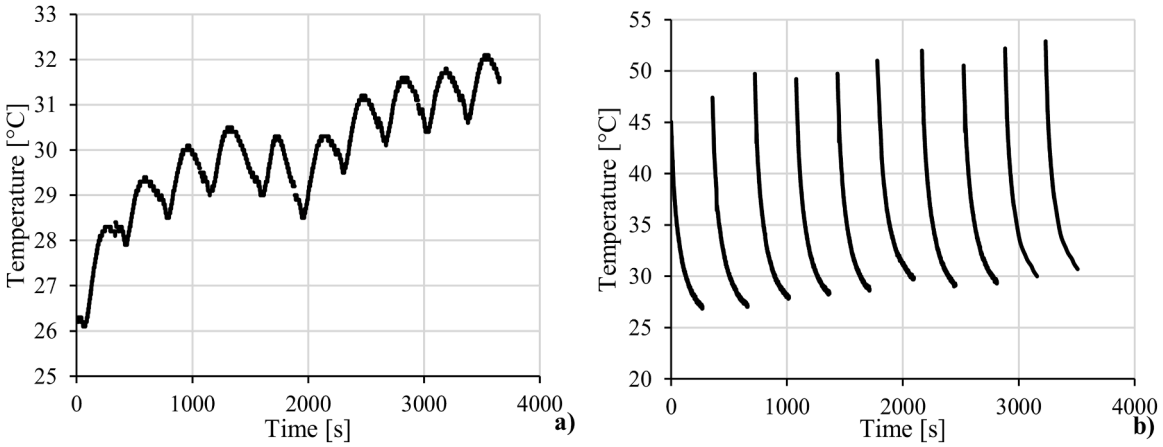

Fig. 6. Volumetric temperature of the mould insert measured by the thermowire a) and the average surface temperature of the mould cavity b) when injection moulding original PP material.

the time-dependent pressure and temperature data are exported from Moldflow to a finite element thermal and mechanical simulation software (Ansys Workbench). There, a transient thermal simulation is created to model the temperature distribution of the mould insert as a function of temperature. The thermal material properties of the injection moulded materials (specific heat, thermal conductivity and density) are needed for accurate modelling of the heat load coming from the product to the mould insert. The heat transfer coefficients were set to 300 W/(m^2• °C) for contacts between the cavity and the product and to 1250 W/(m^2• °C) between the mould components. The heat transfer coefficients between the components in the thermal simulation can only be set properly if measured temperatures are available. It provides the data for the validation of the temperature measurements. It is also essential to properly model the thermal state of the polymeric mould inserts because their stiffness and creep compliance heavily depend on temperature (Figs. 2 and 3). The mechanical simulation therefore requires the temperature-dependent stiffness and creep modulus as inputs. The creep modulus is approximated by the Prony-series method in Ansys Workbench [44].

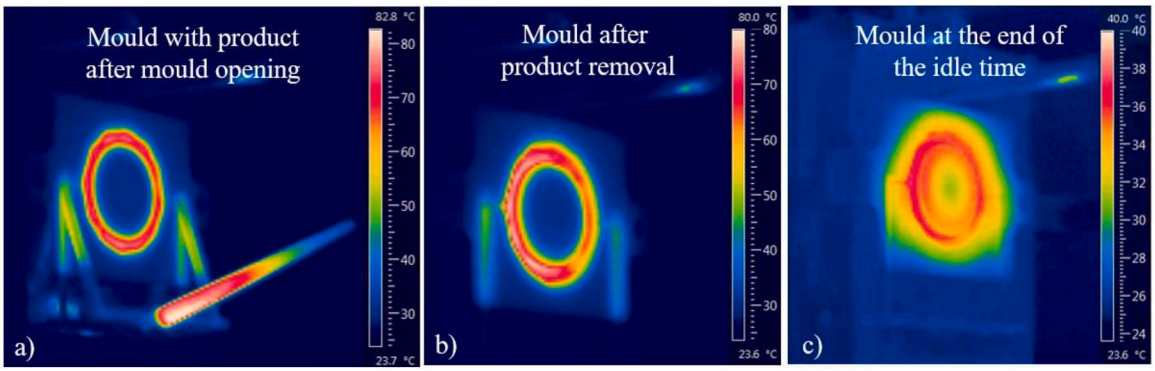

Fig. 7. Surface temperature of the mould cavity and the product when injection moulding of original PP material. The temperature is in °C.

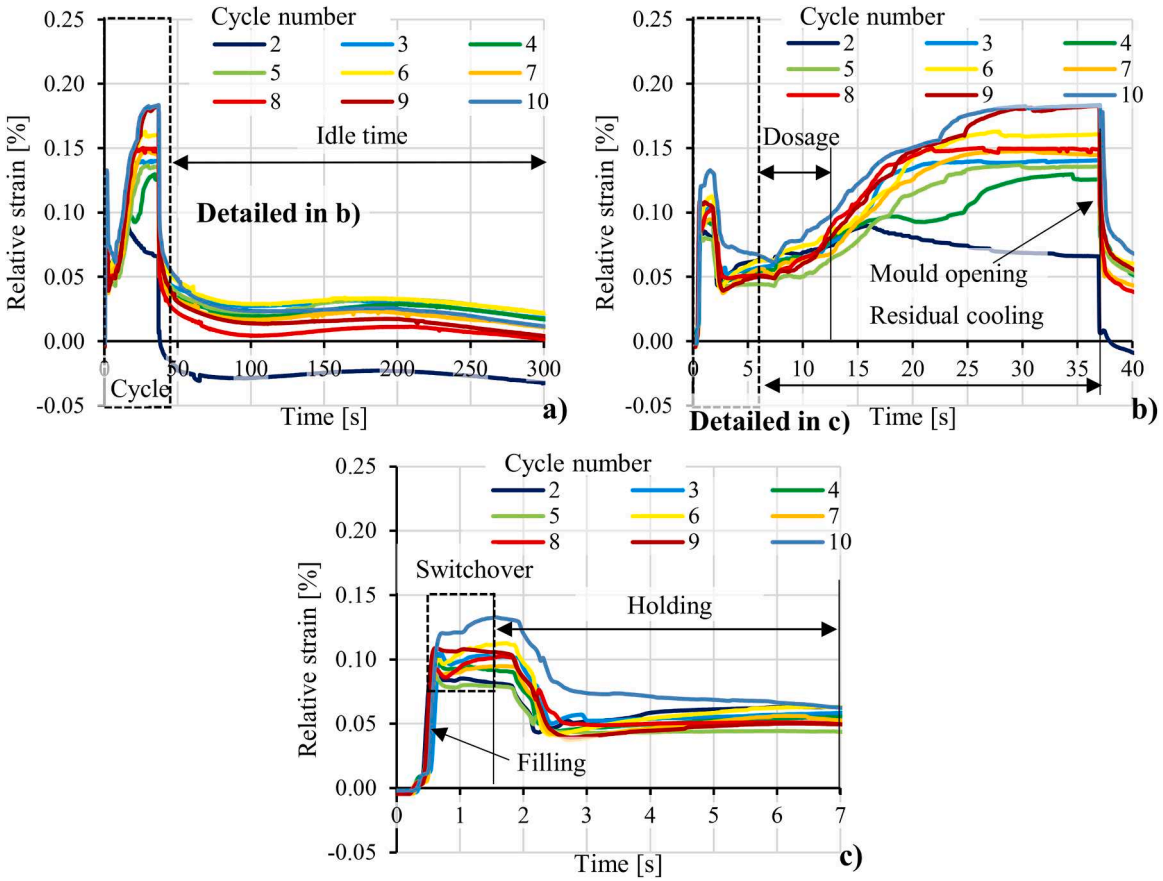

Fig. 8. Operational strain of the mould insert when injection moulding the PP-HDPE mixture. Complete cycle (with delay time) a), moulding cycle from mould closing to part ejection b) and the filling–holding phase c).

3.4.1. Injection moulding simulation

The injection moulding simulation model was built in Autodesk Moldflow Insight. The mould was meshed with three-dimensional 4-node tetrahedron elements. The mesh contained 1 925 966 elements and 366 124 nodes, which was enough to provide the necessary accuracy. The mesh was refined on the cavity surfaces, the part and the mould (especially at the strain gauges and the thermocouple) for improved accuracy of the calculated temperature and strain results. The global edge length of the elements was 4 mm. The mesh of the two mould halves and the moving side mould insert are shown in Fig. 13.

The analysis sequence was Fill + Pack + Warp. The injection moulding parameters were set based on Table 3. The mould mesh, the transient pressure and temperature data were exported from Moldflow with the "mpi2ans" macro. There were 10 time steps in the filling, 10 steps in the holding, and 3 steps in the residual cooling phase. The measured injection pressure–time curves were used to validate the injection moulding simulations. The comparison of the measured injection (machine) pressure–time curves with the simulation is presented in Fig. 14. The injection moulding simulation reproduced the measured curves with adequate accuracy. Slight differences can be seen in the injection pressure curves from 0.5 to 1 s, which can be attributed to the uncertainties of the flow properties (viscosity–shear rate and pressure–specific volume–temperature characteristic) of the moulded materials. The injection pressure of the PP-HDPE mixture exceeded that of the original PP material because of its higher viscosity. Maximum injection pressure was 280 bar for the original PP while it was 405 bar for the PP-HDPE mixture. This increased pressure load in combination with the increased melt temperature caused the elevated deformations when

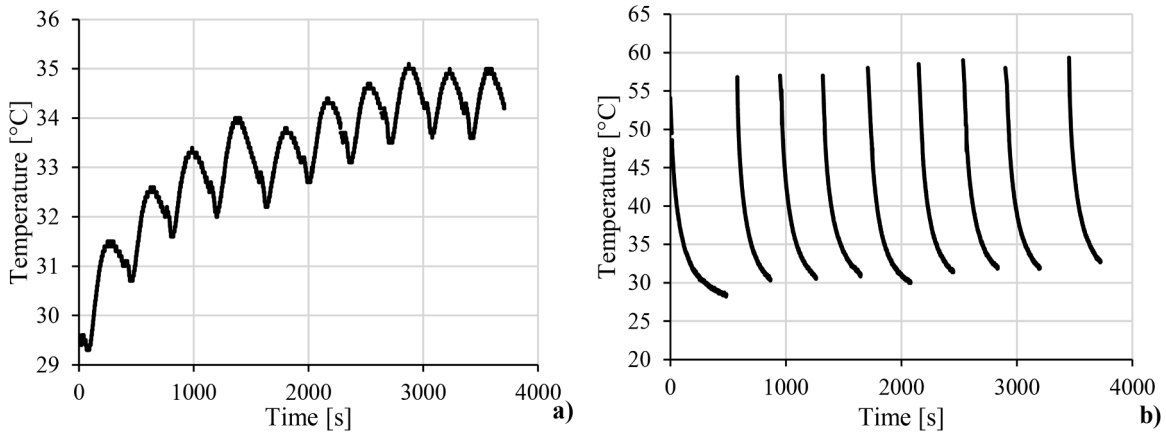

Fig. 9. Volumetric temperature of the mould insert measured by the thermowire and surface temperature of the mould cavity when the PP-HDPE mixture was injection moulded.

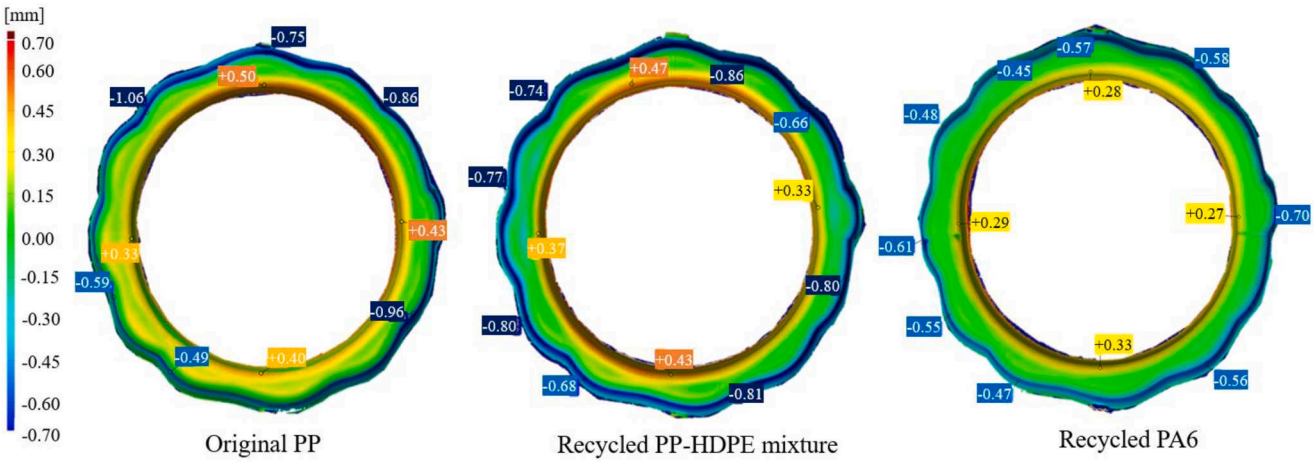

Fig. 10. 3D scanned images of the products injection moulded from the three different materials. Deviations are in mm.

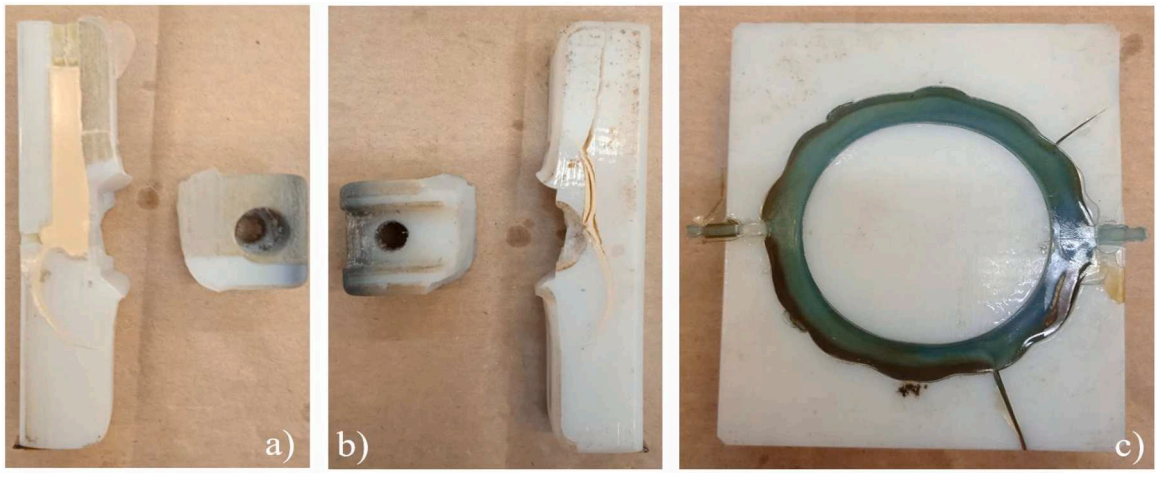

Fig. 11. Failed gate insert (a and b) and the failed mould insert c).

the PP-HDPE mixture was injection moulded.

3.4.3. *Transient thermal simulation*

After the injection moulding simulation, the finite element mesh of the mould and the product were exported from Moldflow to Ansys Workbench, where a transient thermal simulation was prepared. The same mesh was applied in the thermal simulation as in the injection moulding simulation, because the load transfer from Moldflow is based on the node identifiers. It was assumed that the temperature of the injection moulded product remained that of the melt until complete volumetric filling. After that, the product cools down in the cavity until

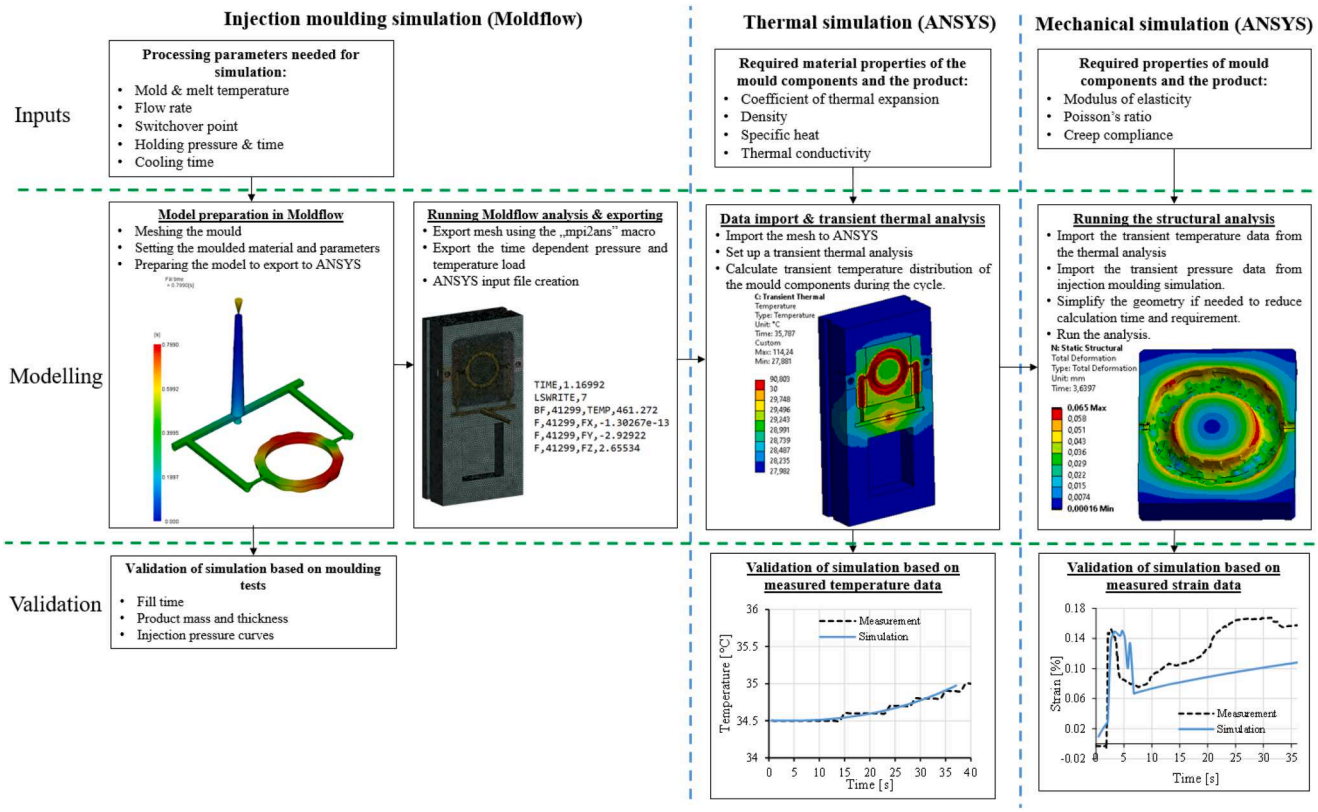

Fig. 12. Flowchart of the simulation process of polymeric mould inserts.

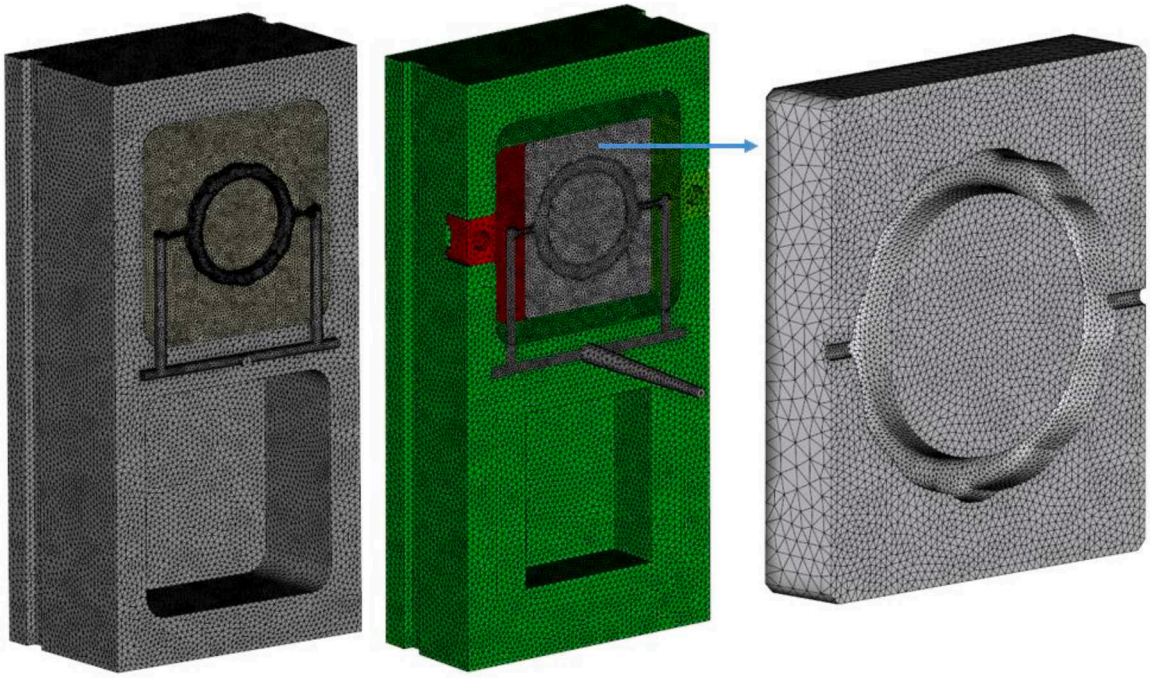

Fig. 13. Finite element mesh of the mould.

mould opening, transferring the heat to the neighbouring mould components. The temperature distribution of the mould block (when injection moulding original PP) is presented at the moment of mould opening in Fig. 15. Heat is localised strictly around the runner and the cavity walls of the additively manufactured gate inserts and the cavity insert.

Fig. 16 shows the temperature distributions of the mould insert at mould opening. The heated zone is localised around the cavity surface because the thermal conductivity of the polymeric insert material (~0.2 W/(m•K)) is approximately two orders of magnitude lower compared to conventional tool steels (typically 20–40 W/(m•K)). The size of the heated zone is the smallest in the case of the original PP material, as the temperature of the injected melt is also the lowest in that case (190 °C).

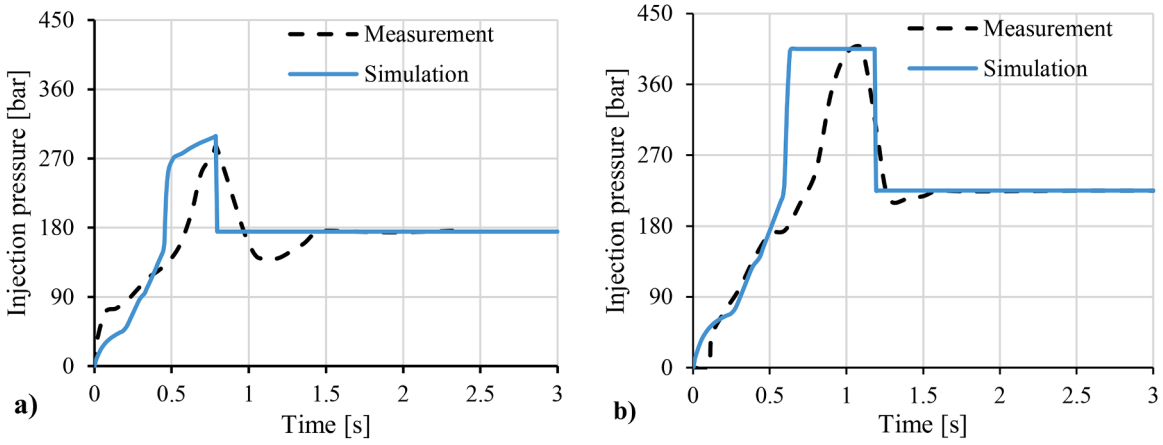

Fig. 14. Comparison of the measured and the calculated injection pressure curves for the original PP a) and the PP-HDPE mixture b).

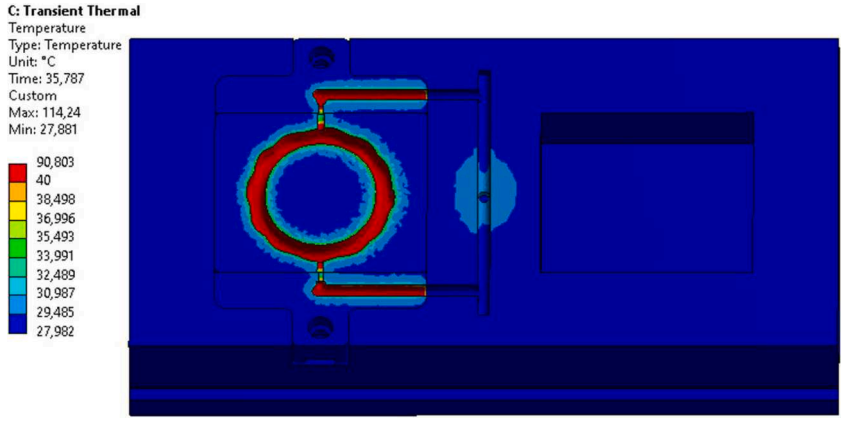

Fig. 15. The temperature distribution of the moving side mould block at the end of the injection moulding cycle. The temperature is in °C.

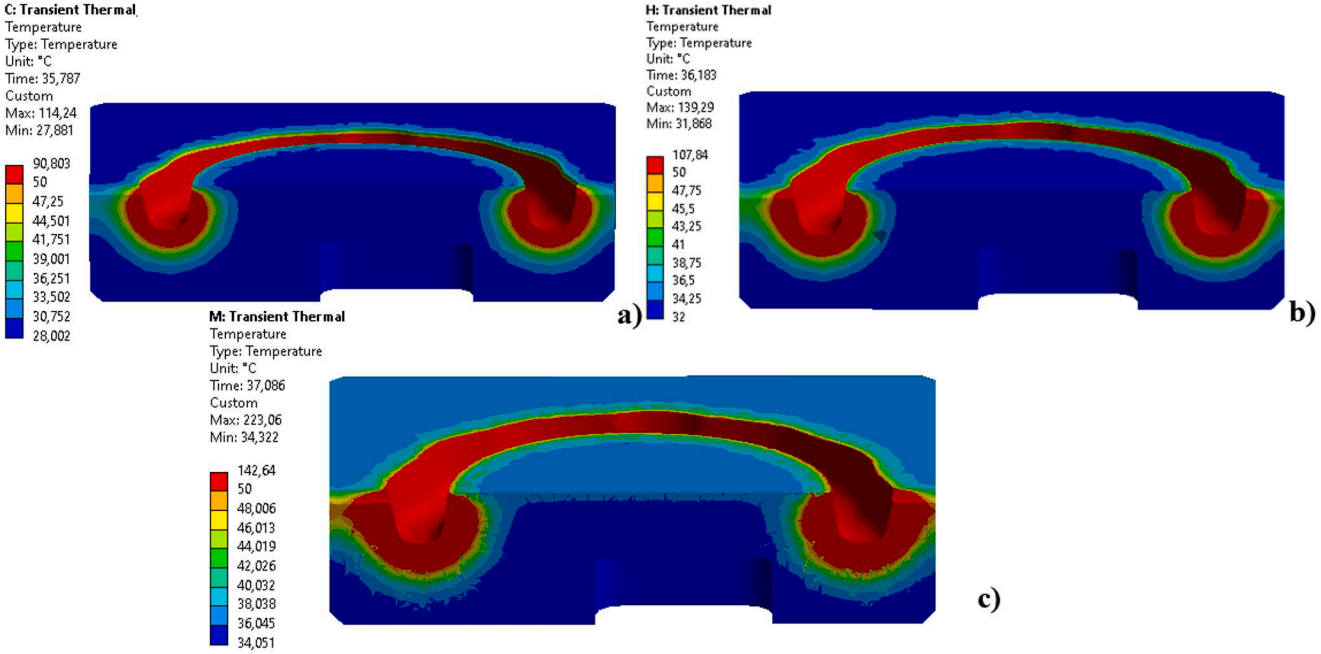

Fig. 16. The temperature distribution of the mould insert at the end of the injection moulding cycle, when injection moulding original PP a), a recycled PP-HDPE mixture b) and recycled PA6 c). The temperature is in °C.

As melt temperature is increased (210 °C for the recycled PP-HDPE mixture and 265 °C for the recycled PA6) the heated zone also expands. These numeric results also prove the experimental assumption that the temperature of the injected melt has a considerable influence on the lifetime of polymeric mould inserts. The dispersion of heat in the mould insert volume is also very slow because of the low thermal conductivity. Due to the significant temperature differences inside the mould insert and the heavy dependence of mechanical properties (stiffness and creep compliance) on temperature, a transient thermal analysis has to be performed for a proper modelling of the temperature field inside the mould insert volume.

The transient thermal simulations were validated based on the volumetric temperatures, measured by the thermowire. The comparison of the measured and the calculated temperature–time curves are presented in Fig. 17 for the three different injection moulded materials. All three materials cause a temperature change of approximately 0.5 °C in the analysed time window (from mould closing to part ejection). Adequate matching can be found between the measured and the calculated temperature–time curves, which proves the accuracy of the simulations. A limitation of the modelling method is that it can only model the steady thermal state of the polymeric mould insert. The cyclic thermal balance is achieved after the first few cycles. The thermal state of a polymeric mould insert profoundly influences the lifetime of the insert. Therefore the long-term performance of the mould can only be estimated if its cyclic thermal behaviour is modelled accurately.

3.4.4. *Static structural simulation*

Following the successful validation of the thermal simulation, we built a structural simulation model to analyse the deformations of the mould insert. This mechanical simulation requires the transient temperature distribution of the mould insert as well as the Poisson's ratio, the temperature dependent stiffness and the creep modulus of the insert material. The creep modulus of the mould insert was approximated with the Prony-series method, while stiffness was approximated with the storage modulus measured by DMA (shown in Fig. 2). The transient pressure load was imported from Moldflow and was represented by a list of nodal forces in each analysed time step. We only analysed the geometry of the mould insert to minimise the required computational effort. "Compression only supports" were used for the surfaces of the mould insert that are in contact with the other mould components or the product. These boundary conditions simulate contact with a perfectly rigid wall, meaning that the mould insert cannot cross this wall but it can detach from it. Fig. 18 shows the deformations after filling and switch-over for the three injection moulded materials, magnified 50 times. The deformed shapes are similar in all cases, as the pressure load acting on the cavity surfaces expands the cavity in all directions. These deformed shapes are in accordance with expectations.

Fig. 19 shows a comparison of the measured directional strains and the simulation results. The operational strains of the mould insert were modelled accurately for all of the three injection moulded materials. Maximum strain was also modelled with excellent accuracy in all of the three analysed cases, which proves the suitability of the coupled simulation method. This modelling method has great practical relevance because low-volume, prototype polymeric injection moulds and mould inserts are gaining popularity in the injection moulding industry. Accurate modelling of their operational behaviour (both thermal and deformational) makes their use easier and more widespread.

4. Conclusions

This article presents a direct rapid tooling approach with additively manufactured moulds to injection mould recycled polymers. This article also presents a coupled simulation approach based on linking injection moulding simulation with finite element thermal and mechanical simulations to model the injection moulding process, the operational temperature distribution and the deformation of the mould inserts. First, material tests (dynamic mechanical analysis in temperature sweep and creep time–temperature superposition mode) were performed to measure the temperature dependence of the stiffness and the creep compliance of the insert material. These data were necessary for subsequent mechanical simulations. The VeroWhite material had a glass transition temperature in the 45–50 °C range. The specific heat–temperature curves of the injection moulded materials were also measured because they were necessary to properly model the heat load acting on the mould insert during the cooling of the injection moulded product. Following the material tests, an injection moulding series was carried out using a PolyJet-printed photopolymer insert. Three different materials were used: original PP, a typical injection moulding grade, a mixture of recycled PP and HDPE (post-consumer cap waste), and recycled PA6 (post-industrial textile waste). The cavity insert endured the test with all of the three different materials (10 cycles with each material) and failed in the first cycle when injection moulding recycled PET (post-consumer bottle waste). The injection moulding series proved that recycled materials can be processed with prototype polymeric injection moulds even when high-performance materials like PA6 are injection moulded. The concept of processing recycled materials with easily customisable and manufacturable low-volume polymeric moulds is a definite novelty.

Following the injection moulding series, we presented a novel finite element modelling method to calculate the operational characteristics of prototype mould inserts. This coupled method consists of modelling the injection moulding cycle first. In this step, the analysed geometry is

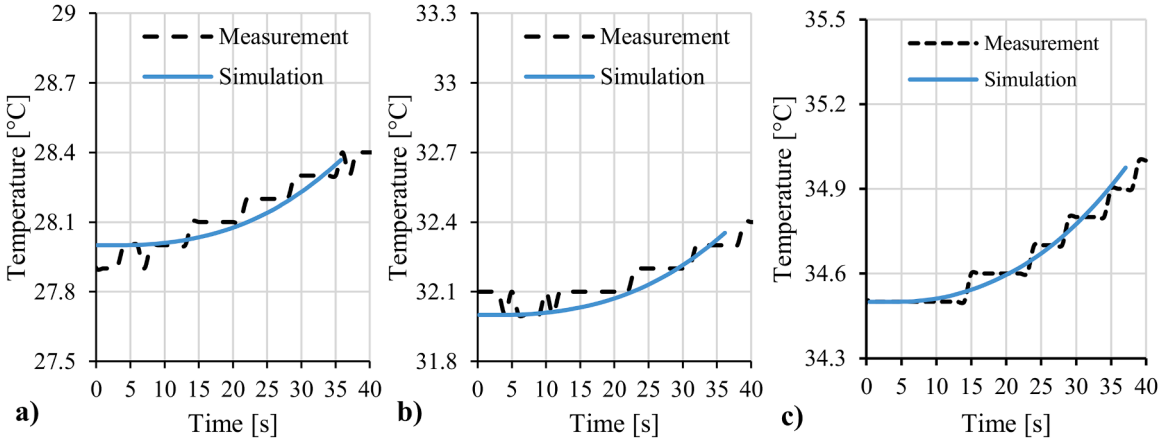

Fig. 17. Comparison of the measured and the simulated volumetric temperatures of the cavity insert when injection moulding original PP a), a recycled PP-HDPE mixture b) and recycled PA6 c).

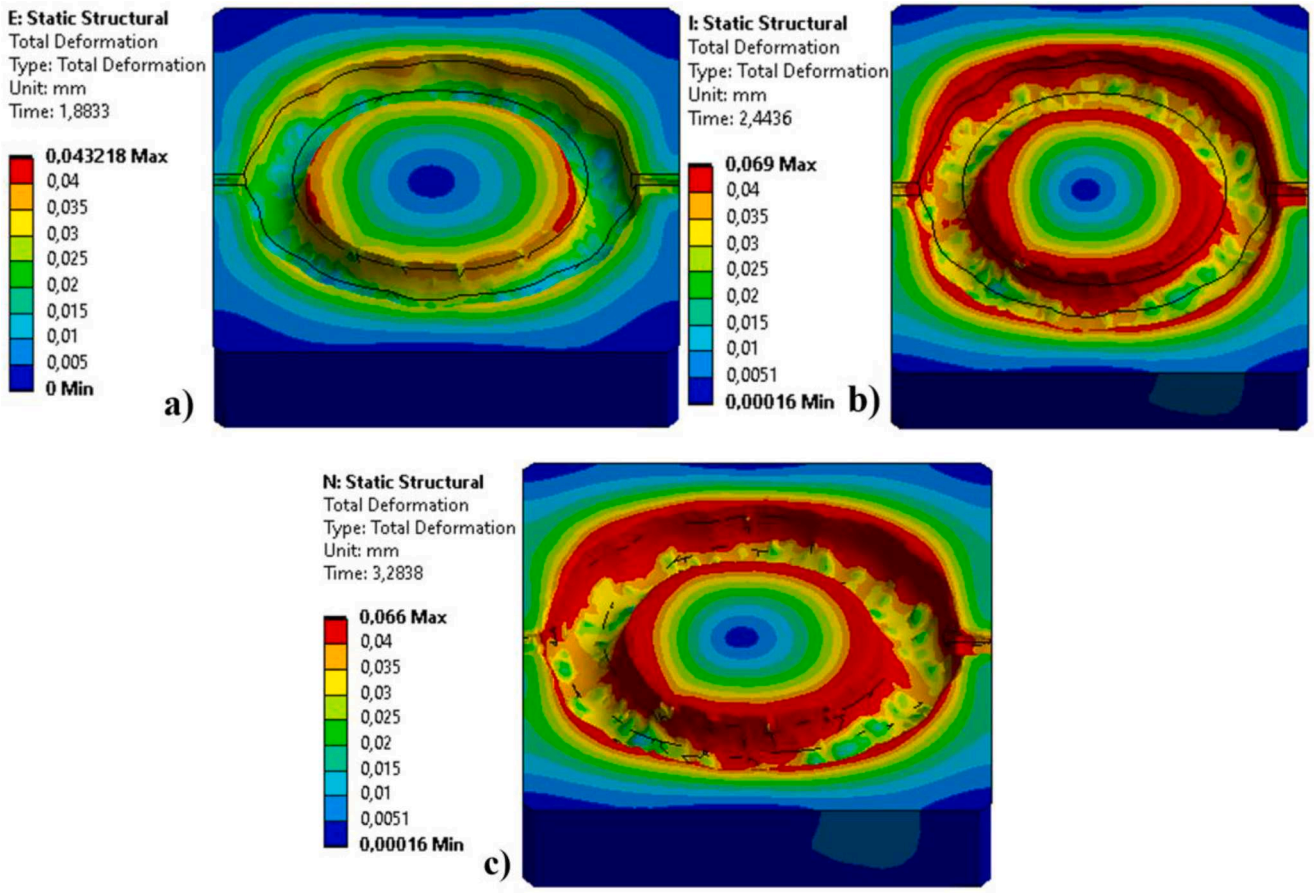

Fig. 18. Maximum deformations of the cavity insert when injection moulding original PP a), recycled PP-HDPE mixture b) and recycled PA6 c). Deformations are in [mm].

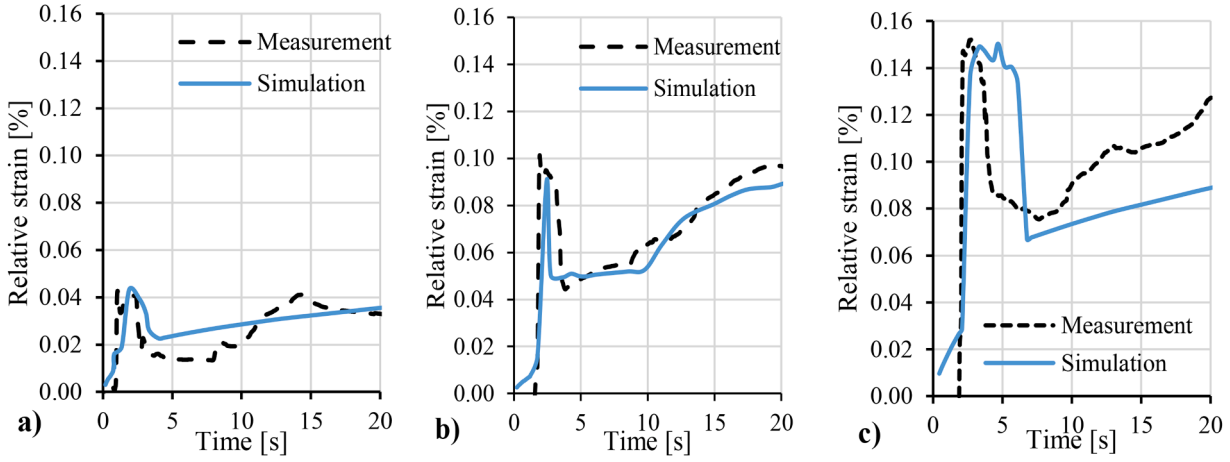

Fig. 19. Comparison of the measured and the calculated operational strains of the cavity insert when original PP a), a recycled PP-HDPE mixture b) and recycled PA6 c) are injection moulded.

meshed and the injection moulding parameters are set, along with the calculation of the fill pattern and the resulting transient pressure distributions. The mesh and the transient pressure results are then exported from the injection moulding simulation. After that, the mesh is imported into a finite element transient thermal simulation, where the cooling of the product and the resulting heating of the mould block is calculated. This transient temperature field has to be accurate as the stiffness, creep compliance and thermal expansion of the mould insert all depend heavily on temperature. In the last step, a mechanical simulation model of the additively manufactured mould insert is built. The finite element mesh of the mould insert and the transient pressure load is imported from the injection moulding simulation and the transient temperature distribution of the mould insert is imported from the thermal simulation. The temperature dependence of the insert material stiffness is set based on the DMA temperature sweep tests, while the creep modulus of the material is modelled with the Prony-series approximation of the DMA creep time temperature superposition tests. The mould insert deformations are then calculated in the finite element mechanical

simulation. Continuous validation of the simulation results is essential during the entire modelling process. In the present article, the injection moulding simulations were validated through the comparison of the measured and the calculated injection (machine) pressure–time curves. Maximum injection pressure was 280 bar in the injection moulding of original PP and 405 bar for the PP-HDPE mixture. The injection moulding simulation showed accurate maximum injection pressures. The transient thermal simulations were compared with the actual volumetric (thermowire) temperature measurements. The mechanical simulation was validated by the strain measurements. Maximum strain at switchover was 0.04 % when PP was injection moulded, 0.10 % when the PP-HDPE mixture was injection moulded, and 0.15 % for PA6. These strain values were accurately reproduced by the simulations. The comparison of the measured and the simulated quantities indicated sufficient accuracy during the entire coupled modelling process. The presented modelling method has significant practical relevance as polymeric moulds and inserts are rapidly gaining ground in the injection moulding industry. This modelling method is a definite novelty and can give a useful tool to design engineers working with polymeric injection moulds or product inserts.

Funding

The research was supported by the National Research, Development and Innovation Office, Hungary (OTKA PD146135 and OTKA FK138501). Project no TKP-6–6/PALY-2021 has been implemented with the support provided by the Ministry of Culture and Innovation of Hungary from the National Research, Development and Innovation Fund, financed under the TKP2021-NVA funding scheme. Project no RRF-2.3.1–21–2022–00,009, titled National Laboratory for Renewable Energy has been implemented with the support provided by the Recovery and Resilience Facility of the European Union within the framework of Programme Széchenyi Plan Plus. The project was funded by the National Research, Development and Innovation Fund of Hungary in the frame of the GINOP_PLUSZ- 2.1.1–21–2022–00,041 project. The research was funded by the Sustainable Development and Technologies National Programme of the Hungarian Academy of Sciences (FFT NP FTA). Dániel Gere is thankful for the János Bolyai Research Scholarship (BO/00,894/23/6) of the Hungarian Academy of Sciences.

Data availability

Data will be made available on request.

CRediT authorship contribution statement

Szabolcs Krizsma: Writing – original draft, Visualization, Validation, Investigation, Formal analysis, Data curation. **András Suplicz:** Writing – review & editing, Writing – original draft, Supervision, Resources, Methodology, Funding acquisition, Conceptualization. **Dániel Gere:** Writing – review & editing, Writing – original draft, Methodology, Investigation, Funding acquisition, Conceptualization.

Declaration of competing interest

The authors declare that they have no known competing financial interests or personal relationships that could have appeared to influence the work reported in this paper.

Acknowledgements

The authors wish to thank ARBURG HUNGÁRIA KFT. for the ARBURG Allrounder injection moulding machine, and TOOL-TEMP HUNGÁRIA KFT., LENZKES GMBH and PIOVAN HUNGARY KFT. for the accessories.

Data availability

Data will be made available on request.

References

[1] S. Rahmati, P. Dickens, Rapid tooling analysis of stereolithography injection mould tooling, Int. J. Mach. Tools Manuf. 47 (2007) 740–747, https://doi.org/10.1016/j.ijmachtools.2006.09.022.
[2] E. Walsh, J.H. ter Horst, D. Markl, Development of 3D printed rapid tooling for micro-injection moulding, Chem. Eng. Sci. 235 (2021) 116498, https://doi.org/10.1016/j.ces.2021.116498.
[3] A. Davoudinejad, M.R. Khosravani, D.B. Pedersen, G. Tosello, Influence of thermal ageing on the fracture and lifetime of additively manufactured mold inserts, Eng. Fail. Anal. 115 (2020) 104694, https://doi.org/10.1016/j.engfailanal.2020.104694.
[4] L. Giorleo, B. Stampone, G. Trotta, Micro injection moulding process with high-temperature resistance resin insert produced with material jetting technology: effect of part orientation, Add. Manuf. 56 (2022) 102947, https://doi.org/10.1016/j.addma.2022.102947.
[5] L. Bogaerts, M. Faes, J. Bergen, J. Cloots, E. Vasiliauskaite, F. Vogeler, D. Moens, Influence of thermo-mechanical loads on the lifetime of plastic inserts for injection moulds produced via additive manufacturing, Procedia CIRP 96 (2021) 109–114, https://doi.org/10.1016/j.procir.2021.01.061.
[6] A. Bagalkot, D. Pons, D. Symons, D. Clucas, Categorization of failures in polymer rapid tools used for injection molding, Processes 7 (2019) 17, https://doi.org/10.3390/pr7010017.
[7] B. Stampone, K.I. Deniz, A. Foscarini, A. Turco, M.S. Chiriacò, F. Ferrara, L. Giorleo, G. Trotta, Rapid tooling for microinjection moulding of proof-of-concept microfluidic device: resin insert capability and preliminary validation, Appl. Sci. 14 (2024) 3157, https://doi.org/10.3390/app14083157.
[8] A. Bagalkot, D. Pons, D. Clucas, D. Symons, A methodology for setting the injection moulding process parameters for polymer rapid tooling inserts, Rapid. Prototyp. J. 25 (2019) 1493–1505, https://doi.org/10.1108/rpj-10-2017-0217.
[9] C. Berges, J. Hidalgo, R. Andújar, R. Campana, G. Herranz, Prospects of producing solid oxide fuels interconnectors processed by metal injection moulding, Resul. Eng. 11 (2021) 100268, https://doi.org/10.1016/j.rineng.2021.100268.
[10] G.A. Mendible, J.A. Rulander, S.P. Johnston, Comparative study of rapid and conventional tooling for plastics injection molding, Rapid Prototyp. J. 23 (2017) 344–352, https://doi.org/10.1108/rpj-01-2016-0013.
[11] G.A. Mendible, N. Saleh, C. Barry, S.P. Johnston, Mechanical properties and crystallinity of polypropylene injection molded in polyjet and aluminum tooling, Rapid. Prototyp. J. 28 (2022) 686–694, https://doi.org/10.1108/rpj-09-2020-0221.
[12] A. Kampker, J. Triebs, S. Kawollek, P. Ayvaz, T. Beyer, Direct polymer additive tooling – effect of additive manufactured polymer tools on part material properties for injection moulding, Rapid Prototyp. J. 25 (2019) 1575–1584, https://doi.org/10.1108/rpj-07-2018-0161.
[13] T. Tábi, N.K. Kovács, I.E. Sajó, T. Czigány, S. Hajba, J.G. Kovács, Comparison of thermal, mechanical and thermomechanical properties of poly(lactic acid) injection-molded into epoxy-based Rapid Prototyped (PolyJet) and conventional steel mold, J. Therm. Anal. Calorim. 123 (2016) 349–361, https://doi.org/10.1007/s10973-015-4997-y.
[14] J. Bobek-Nagy, R. Kurdi, A. Kovács, L. Simon-Stőger, M. Szigeti, C. Varga, How introduction of deposit-refund system (DRS) changes recycling of non-drinking bottle PET wastes, Express Polym. Lett. 17 (2023) 1166–1179, https://doi.org/10.3144/expresspolymlett.2023.88.
[15] F. Ronkay, D. Gere, E. Slezák, E. Szabó, G. Marosi, K. Bocz, Recycled PET packaging materials of improved toughness— Importance of devitrification of the rigid amorphous fraction, Macromol. Mater. Eng. (2024) 2400219, https://doi.org/10.1002/mame.202400219.
[16] A. Toldy, Challenges and opportunities of polymer recycling in the changing landscape of European legislation, Express Polym. Lett. 17 (2023) 1081, https://doi.org/10.3144/expresspolymlett.2023.81.
[17] K. Ragaert, L. Delva, K. Van Geem, Mechanical and chemical recycling of solid plastic waste, Waste Manag. 69 (2017) 24–58, https://doi.org/10.1016/j.wasman.2017.07.044.
[18] F. Ronkay, B. Molnar, D. Gere, T. Czigany, Plastic waste from marine environment: demonstration of possible routes for recycling by different manufacturing technologies, Waste Manag. 119 (2021) 101–110, https://doi.org/10.1016/j.wasman.2020.09.029.
[19] G. Kónya, P. Ficzere, The effect of layer thickness and orientation of the workpiece on the micro- and macrogeometric properties and the machining time of the part during 3D printing, Period. Polytechn. Mech. Eng. 67 (2023) 143–150, https://doi.org/10.3311/PPme.21473.
[20] L. Tóth, E. Slezák, K. Bocz, F. Ronkay, Progress in 3D printing of recycled PET, Mater. Today Sust. 26 (2024) 100757, https://doi.org/10.1016/j.mtsust.2024.100757.
[21] K. Mikula, D. Skrzypczak, G. Izydorczyk, J. Warchoł, K. Moustakas, K. Chojnacka, A. Witek-Krowiak, 3D printing filament as a second life of waste plastics-a review, Environ. Sci. Pollut. Res. 28 (2021) 12321–12333, https://doi.org/10.1007/s11356-020-10657-8.

[22] A.L. Woern, J.R. McCaslin, A.M. Pringle, J.M. Pearce, RepRapable Recyclebot: open source 3-D printable extruder for converting plastic to 3-D printing filament, HardwareX 4 (2018) e00026, https://doi.org/10.1016/j.ohx.2018.e00026.
[23] A. Romani, M. Levi, J.M. Pearce, Recycled polycarbonate and polycarbonate/acrylonitrile butadiene styrene feedstocks for circular economy product applications with fused granular fabrication-based additive manufacturing, Sust. Mater. Technol. 38 (2023) e00730, https://doi.org/10.1016/j.susmat.2023.e00730.
[24] S. Krizsma, A. Suplicz, Comprehensive in-mould state monitoring of Material Jetting additively manufactured and machined aluminium injection moulds, J. Manuf. Process. 84 (2022) 1298–1309, https://doi.org/10.1016/j.jmapro.2022.10.070.
[25] S. Krizsma, N.K. Kovács, J.G. Kovács, A. Suplicz, In-situ monitoring of deformation in rapid prototyped injection molds, Add. Manuf. 42 (2021) 102001, https://doi.org/10.1016/j.addma.2021.102001.
[26] T. Ageyeva, S. Horváth, J.G. Kovács, In-mold sensors for injection molding: on the way to industry 4.0, Sensors 19 (2019) 3551, https://doi.org/10.3390/s19163551.
[27] N.-Y. Zhao, J.-F. Liu, M.-Y. Su, Z.-B. Xu, Measurement techniques in injection molding: a comprehensive review of machine status detection, molten resin flow state characterization, and component quality adjustment, Measurement 226 (2024) 114163, https://doi.org/10.1016/j.measurement.2024.114163.
[28] J.-Y. Chen, J.-X. Zhuang, M.-S. Huang, Enhancing the quality stability of injection molded parts by adjusting V/P switchover point and holding pressure, Polymer 213 (2021) 123332, https://doi.org/10.1016/j.polymer.2020.123332.
[29] R. Mahshid, Y. Zhang, H.N. Hansen, A.H. Slocum, Effect of mold compliance on dimensional variations of precision molded components in multi-cavity injection molding, J. Manuf. Process. 67 (2021) 12–22, https://doi.org/10.1016/j.jmapro.2021.04.048.
[30] M.-S. Huang, C.-Y. Lin, A novel clamping force searching method based on sensing tie-bar elongation for injection molding, Int. J. Heat Mass Transf. 109 (2017) 223–230, https://doi.org/10.1016/j.ijheatmasstransfer.2017.02.004.
[31] M. Gülçür, P. Wilson, M. Donnelly, K. Couling, V. Goodship, J. Charmet, M. A. Williams, G. Gibbons, X-ray computed tomography for predictive quality assessment, 3D visualisation of micro-injection mouldings and soft-tool deformation, Mater. Des. 227 (2023) 111741, https://doi.org/10.1016/j.matdes.2023.111741.
[32] F. Baruffi, M. Gülçür, M. Calaon, J.-M. Romano, P. Penchev, S. Dimov, B. Whiteside, G. Tosello, Correlating nano-scale surface replication accuracy and cavity temperature in micro-injection moulding using in-line process control and high-speed thermal imaging, J. Manuf. Process. 47 (2019) 367–381, https://doi.org/10.1016/j.jmapro.2019.08.017.
[33] P. Guerrier, G. Tosello, J.H. Hattel, Flow visualization and simulation of the filling process during injection molding, CIRP J. Manuf. Sci. Technol. 16 (2017) 12–20, https://doi.org/10.1016/j.cirpj.2016.08.002.
[34] B. Abbès, F. Abbès, H. Abdessalam, A. Upganlawar, Finite element cooling simulations of conformal cooling hybrid injection molding tools manufactured by selective laser melting, Int. J. Adv. Manuf. Technol. 103 (2019) 2515–2522, https://doi.org/10.1007/s00170-019-03721-2.
[35] J.-S. Huang, C.-Y. Wang, Numerical simulation and measurement of effective thermal conductivity of an additively manufactured lattice microstructure with gradient porosity, Resul. Eng. 25 (2025) 104177, https://doi.org/10.1016/j.rineng.2025.104177.
[36] M.B. Slama, S. Chatti, A. Chaabene, K. Ghozia, H.Z. Touati, Design for additive manufacturing of plastic injection tool inserts with maintenance and economic considerations: an automotive study case, J. Manuf. Process 102 (2023) 765–779, https://doi.org/10.1016/j.jmapro.2023.07.070.
[37] F.J. Cervantes-Vallejo, C. Hernández-Navarro, K.A. Camarillo-Gómez, J.F. Louvier-Hernández, J. Navarrete-Damián, Thermal-structural optimization of a rapid thermal response mold: comprehensive simulation of a heating rod system and a fluid cooling system implemented MSR-PSO-FEM, Thermal Sci. Eng. Progr. 47 (2024) 102279, https://doi.org/10.1016/j.tsep.2023.102279.
[38] C. Macedo, A.M. Brito, L. Faria, C.L. Simões, J. Laranjeira, R. Simoes, The potential of RHCM technology in injection molding using a simple convention heating and cooling system, Resul. Eng. 19 (2023) 101349, https://doi.org/10.1016/j.rineng.2023.101349.
[39] L. Crema, M. Sorgato, G. Lucchetta, Thermal optimization of deterministic porous mold inserts for rapid heat cycle molding, Int. J. Heat Mass Transf. 109 (2017) 462–469, https://doi.org/10.1016/j.ijheatmasstransfer.2017.02.023.
[40] G.-L. Wang, G.-Q. Zhao, X.-X. Wang, Heating/cooling channels design for an automotive interior part and its evaluation in rapid heat cycle molding, Mater. Des. 59 (2014) 310–322, https://doi.org/10.1016/j.matdes.2014.02.047.
[41] C.-L. Xiao, H.-X. Huang, Development of a rapid thermal cycling molding with electric heating and water impingement cooling for injection molding applications, Appl. Therm. Eng. 73 (2014) 712–722, https://doi.org/10.1016/j.applthermaleng.2014.08.027.
[42] X.-P. Li, N.-N. Gong, Y.-J. Guan, G.-M. Cheng, Thermal and stress analysis of rapid electric heating injection mold for a large LCD TV panel, Appl. Therm. Eng. 31 (2011) 3989–3995, https://doi.org/10.1016/j.applthermaleng.2011.07.050.
[43] P. Guerrier, G. Tosello, K.K. Nielsen, J.H. Hattel, Three-dimensional numerical modeling of an induction heated injection molding tool with flow visualization, Int. J. Adv. Manuf. Technol. 85 (2016) 643–660, https://doi.org/10.1007/s00170-015-7955-8.
[44] ANSYS Workbench Mechanical 2019 Help- Chapter 4.9. Viscoelasticity.